N89-22911

A MAGNETIC DAMPER FOR FIRST MODE VIBRATION REDUCTION IN MULTIMASS FLEXIBLE ROTORS

M.E.F. Kasarda
Rotor Bearing Dynamics, Inc.
Wellsville, New York 14895, U.S.A.

P.E. Allaire, R.R. Humphris, and L.E. Barrett
Department of Mechanical and Aerospace Engineering
University of Virginia
Charlottesville, Virginia 22901, U.S.A.

Many rotating machines such as compressors, turbines and pumps have long thin shafts with resulting vibration problems. They would benefit from additional damping near the center of the shaft. Magnetic dampers have the potential to be employed in these machines because they can operate in the working fluid environment unlike conventional bearings. This paper describes an experimental test rig which was set up with a long thin shaft and several masses to represent a flexible shaft machine. An active magnetic damper was placed in three locations: near the midspan, near one end disk, and close to the bearing. With typical control parameter settings, the midspan location reduced the first mode vibration 82%, the disk location reduced it 75% and the bearing location attained a 74% reduction. Magnetic damper stiffness and damping values used to obtain these reductions were only a few percent of the bearing stiffness and damping values. A theoretical model of both the rotor and the damper was developed and compared to the measured results. The agreement was good.

NOMENCLATURE

Symbol	Meaning
A	Area of magnetic pole face (one)
C	Capacitance
c_{eq}	Equivalent damping
F	Force
G	Controller transfer function
h	Gap thickness
h_s	Steady state gap thickness
i	Current
i_s	Steady state current
i_b	Bottom magnet current
i_t	Top magnet current
K_a	Current amplifier gain

K_{eq}	Equivalent stiffness
K_g	Proportional gain
K_i	Current stiffness
K_g	Rate gain
K_t	Controller total gain
K_y	Position stiffness
M	Mass
N	Number of turns (per leg)
R	Resistance
s	Laplace variable
W	Weight
y	Vertical position
ω	Angular velocity
ϕ	Magnetic flux
μ_o	Permeability of free space
τ	Time constant

INTRODUCTION

Compressors, turbines and other rotating machines often have long thin shafts which give rise to high vibration problems. Currently, many compressors operate above the first [1] or second critical speed. Steam turbines also operate above several critical speeds. Seals inside compressors give rise to cross coupled stiffness terms which may drive a machine into large subsynchronous vibrations [2]. Nicholas et al. [3] report on the effects of flexible supports which tend to increase vibration levels in steam turbines. Generally it is desirable to increase the damping effects near the center of these long, thin shaft machines. One method of doing this is to place a damper inside the machine casing.

The concept of using a damper inside these machines is not new. Such a damper would be located somewhere between the bearings and apply damping, and perhaps stiffness, to the rotor. What has been lacking until recent years is a damper which could operate in the environment of the working fluid. Conventional rolling element and fluid film bearings require an oil supply. A central damper in a compressor would have to be sealed so that the oil does not contaminate the gas. In most cases, the additional complications do not warrant the damper. In steam turbines, the temperature is so high that an oil damper could not be used inside the turbine.

Magnetic dampers are now a real possibility for these types of machines. Commercial magnetic bearings [4,5] are increasingly being used for compressors and other machines. These do not require oil and can operate at high temperatures, thus removing the limitations indicated above. To date, the authors are not aware of the use of a magnetic damper in a field application in North America.

A magnetic bearing can be used as a magnetic damper simply by having it carry no load. Thus the machine is completely supported in regular bearings. Typically these are oil lubricated bearings. If the damper is not active, then the machine reverts to its normal behavior without a damper effect. Some early work on simple rotors with active control was reported in [6,7] by Allaire et al.

Several studies have been carried out by Holmes et al.[8,9] on the suppression of vibrations in long transmission shafts. A magnetic damper was placed at various locations along the shaft to determine the reduction. These studies differ from the present paper because there were no large masses located along the shaft such as occur in compressors and turbines.

A magnetic bearing/damper has been developed at the University of Virginia. It was used as the damper in this work, so the relevant publications are described in some detail here. The basic bearing geometry and control algorithm was described by Humphris et al. [10]. The effects of the bearing employed to support a flexible rotor were measured and reported in Allaire et al. [11-13]. Adjustment of the bearing stiffness properties via the control system gains allowed movement of the rotor first critical speed from approximately 800 rpm to 2,000 rpm, which is more than a factor of two. Variation of the bearing damping properties gave a reduction in rotor vibrations of as much as an order of magnitude. The first results using the magnetic bearing as a damper (not supporting any steady state load) were reported in [14]. Also, initial results of employing digital control to operate magnetic bearings were published in [15].

The purpose of this paper is to report on the use of an active magnetic damper in a multimass flexible rotor. Three large disks were placed on a shaft, supported in conventional bearings, to represent a multimass compressor or steam turbine. The magnetic damper was placed in various locations to observe the vibration reduction capabilities. The magnetic damper was placed near the midspan, near one end disk, and as close to the outboard bearing as possible.

ACTIVE MAGNETIC DAMPER

An active magnetic damper is essentially an active magnetic bearing with no load support capacity. The magnetic damper used in this analysis consists of four electromagnets located radially around the rotor shaft. The electromagnet currents, which determine the force in each magnet, were determined by a controller which maintained the shaft in the center of the damper by continuously monitoring the shaft position and adjusting the electromagnet currents accordingly. There were air gaps between the shaft and the magnets and the shaft did not contact the magnets. The dynamic properties of the damper (i.e. damping and stiffness) were electronically regulated by the controller.

A diagram of the four electromagnets which made up the damper is shown in Figure 1. They were located radially around a laminated ferromagnetic disk which was attached to the rotor shaft. The purpose of this laminated disk was to provide a continuous flux path between the magnet pole faces with a minimum of eddy current losses.

Each electromagnet in the damper consisted of a solid soft iron core forming a horseshoe, with two pole faces cut to a diameter of 60.5 mm (2.38 inches). This gave a nominal radial clearance of 1.0 mm (0.040 inches). Each leg of the coil was wound with 920 turns of wire. All electromagnets were the same with equal steady state currents. Presented in appendix A is the theory of the damper characteristics.

Two proximitor (eddy current) probes located vertically and horizontally near the damper (unless otherwise specified) were used as rotor position sensors for input

to the electronic controller. Various tests were previously conducted to insure that the magnetic fields from the damper did not affect the readings of the probes.

TEST RIG

A four mass laboratory rotor was constructed with a 19.0 mm (0.75 inch) shaft supported in conventional sleeve bearings with a bearing span of 660.4 mm (26.0 inches). Three steel disks were placed four inches apart at the center of the shaft leaving 190.5 mm (7.5 inches) between each outboard disk and the closest support bearing. Each of these three disks was 139.7 mm (5.5 inches) in diameter, 25.4 mm (1.0 inch) in thickness, and weighed 28.48 N (6.4 lbs). The fourth mass was the laminated ferromagnetic damper disk which weighed 4.90 N (1.1 lbs) and was 58.4 mm (2.3 in) in diameter with a thickness of 25.4 mm (1.0 inch). The total rotor length and weight, including the laminated magnetic disk, was 762 mm (30.0 inches) and 107.2 N (24.1 lb), respectively.

This damper disk was placed at three different locations on the rotor, illustrated in Figure 2, depending on the desired location of the magnetic damper. The three locations were at the midspan near the center disk, near the third disk at the quarterspan of the rotor, and at a location just inboard of the outer bearing. These locations were chosen to demonstrate the effect of a damper at optimum and less than optimum rotor locations for control of one or more modes of vibration. These locations represent situations where there may be design constraints on an actual machine as to the placement of a magnetic damper on the rotor. As shown in Figure 2, shaft displacement sensors were placed at 3 different locations to monitor shaft motion. These locations will be referred to from left to right as the disk 1 probe, midspan probe and disk 3 probe, respectively. The four mass rotor will now be referred to as the 3-mass rotor, due to the relatively small mass of the laminated ferromagnetic disk compared to the three large steel disk masses.

The 3-mass rotor was attached to an aluminum baseplate which was fixed to a large concrete block by anchor bolts. Shim stock was placed underneath the aluminum baseplate to correct a slight bow in the baseplate. The shaft was also twisted (bowed) with a significant shaft bow which could not be corrected. For example, when the shaft bow at the midspan probe was reduced to below .0254 mm (1 mil), the bow near the first disk was still close to .0508 mm (2 mils).

The rotor was driven by a 1/2 hp electric motor which was rated at 10,000 RPM. The motor transmitted power through a flexible rubber coupling as shown in Figure 2.

A total of three vertical and three horizontal proximitor probes were used to monitor shaft displacements. A separate proximitor probe was used as a key phasor. Signals from the probes were run to two digital vector filters, where amplitude and phase information at the probes was determined. One set of proximitor probes was also used as input sensors for the magnetic damper controller. These sensors were always located close to the damper.

The three-mass experimental rotor was used to study the effects of a magnetic damper located at the three locations on the shaft. The magnetic damper, used in conjunction with a controller, exhibited some nonlinear effects above 4,000 RPM. Therefore this paper will be limited to operation below 4000 RPM (66.7 Hz). The first rotor bending mode is located at about 1600 RPM (26.7 Hz), with all other modes located at frequencies greater than 4000 RPM (66.7 Hz).

DAMPER AT MIDSPAN

The first location of the magnetic damper to be investigated was the midspan location as shown in Figure 2a. This was expected to be the optimum position for control of first mode vibrations.

The effect of increasing rate gain (K_r) or damping and proportional gain (K_g) or stiffness of the electromagnetic damper was studied at each location. The rate gain (K_r) was varied from a nominal value of 2.0 to a maximum value of 20.0. Due to stability problems, it was not possible to use this damper with pure damping or rate gain (K_r), and therefore, the controller was set with a nominal proportional gain (K_g) of 2.5, while the rate gain (K_r) was varied for analysis. Similarly, the electromagnetic damper could not be used with pure stiffness or proportional gain (K_g), and the controller was set with a nominal rate gain (K_r) of 5.0 while the proportional gain (K_g) was varied from 2.5 to 10.0. Finally, a comparison of the effect of the damper location for fixed values of rate gain (K_r) and proportional gain (K_g) was carried out.

The effect of using the damper at the midspan is shown in Figure 3. The rotor was run with the damper off and with rate gain (K_r) equal to 2.0, 5.0 and 10.0. Proportional gain was held constant at 2.5. There was an 82% reduction in amplitude with a rate gain of 10.0 over the case with the damper off.

An unbalance response model of the rotor was developed to compare to the measured data. Stiffness and damping coefficients were evaluated for the damper as described in Appendix B. Also, the unbalance level in the rotor was determined by balancing the rotor to a low level and then adding a known unbalance weight in the center disk.

The forced response predictions for the magnetic damper at the midspan of the 3-mass rotor are plotted in Figure 4 for cases with the magnetic damper off, and with the damper on with a rate gain (K_r) equal to 2.0, 5.0, and 10.0, respectively. A maximum reduction of 88% in the amplitude of vibration occurs theoretically with $K_r = 10$ as compared to the value of 82% for the measured case.

It may be seen from these results that even a small amount of damping can greatly reduce the vibration level. For $K_r = 2.0$, the estimated damping value was 31 N-sec/m (0.18 lb-sec/in), which produces a 49% decrease in amplitude at the rotor center. The estimated bearing damping was 1050 N-sec/m (6.0 lb-sec/in). Thus the actual midspan damping is only approximately 3% of the bearing damping. At $K_r = 10$, the estimated damping was 122 N-sec/m (0.70 lb-sec/in) or approximately 12% of the bearing damping. This produced an 82% reduction in amplitudes of vibration.

Figure 5 shows the experimental values for the midspan damper location as the proportional gain (K_g) had the values 2.5, 5.0 and 7.5. The rate gain was held constant at $K_r = 5.0$. The critical speed increased from 1600 rpm (26.7 Hz) to 2570

rpm (42.8 Hz) with K_g = 7.5. The value of K_g = 7.5 corresponds to a damper stiffness of 210,000. N/m (1200 lb/in). This stiffness value is only about 10% of the bearing vertical stiffness.

The calculated forced response is shown in Figure 6. The predicted increase in critical speed is 38% for K_g = 7.5. This is somewhat lower than the 60% measured increase in critical speed. Also, the theory predicted a steady increase in amplitude with increasing K_g, whereas the measured values decreased and then increased. Overall, however, the agreement is good.

DAMPER AT DISK THREE

The second location of the magnetic damper is the disk three location as shown in Figure 2. This was expected to be the next best position for control of the first mode vibrations.

The effect of using the damper at disk three is shown in Figure 7. The rotor was run with the damper off and the rate gain (K_r) equal to 5.0, 10.0, and 20.0. Proportional gain was held constant at 2.5. There is a 75% reduction in amplitude with a rate gain of 20.0 over the case with the damper off.

An unbalance response model of the rotor with the damper at disk three was also developed for comparison with the measured data. The forced response predictions for this configuration are plotted in Figure 8 for cases with the magnetic damper off, and with the damper on, with a rate gain (K_r) equal to 5.0, 10.0, and 20.0, respectively. A maximum reduction of 85% in the amplitude of vibration occurred theoretically with K_r = 20, as compared to the value of 75% for the measured case.

Again, it may be seen from these results that even a small amount of damping can greatly reduce the vibration level. At K_r = 20, the estimated damping was 175 N-sec/m (1.0 lb-sec/in) or 17% of the bearing damping. This produced a 75% reduction in amplitudes of vibration.

Experimental data was also taken for the disk three damper location with proportional gain (K_g) values of 2.5, 7.5, and 10.0, while the rate gain (K_r) remains at 5.0. The critical speed increased from 1600 RPM (26.7 Hz) to 1920 RPM (32 Hz) with K_g = 10.0. The value of K_g = 10.0 corresponded to a damper stiffness of 262,000 (1500 lb/in). This stiffness value was only about 13% of the bearing vertical stiffness.

The corresponding forced response calculations predicted a 25% increase in the critical speed frequency for K_g = 10.0. This was somewhat higher than the measured value of 19%. Once again the theory predicted a steady increase in amplitude with increasing K_g whereas the measured values decreased and then increased. In general, however, the agreement was good.

DAMPER AT BEARING

The third location of the magnetic damper to be investigated was the bearing location as shown in Figure 2c. This was expected to be the least effective location for control of the first mode of vibrations.

The effect of using the damper at the bearing was similar to the effect of the damper at other locations. However, experimental data was taken for the rotor when the rate gain (K_r) was equal to 5.0, 10.0, and 20.0, while the proportional gain (K_g) equals 2.5. There was a significant 74% reduction in amplitude with a rate gain of 20.0, over the case with the damper off whereas forced response calculations predicted only a 52% decrease.

Similar data was taken when the proportional gain (K_g) was set at 2.5, 7.5, and 10.0, with the rate gain (K_r) equal to 5.0. There was a measured 11% increase in the first critical speed from 1620 RPM (27 Hz) with the damper off to 1800 RPM (30 Hz) with the proportional gain (K_g) equal to 10.0. Forced response calculations predicted a 6% increase in critical speed.

EFFECT OF MAGNETIC DAMPER LOCATION

A summary of the measured effect of magnetic damper location is shown in Figure 9, when the proportional gain (K_g) equals 2.5 and the rate gain (K_r) equals 5.0. As noted, the optimum control of the first mode vibrations occurs when the damper is at the midspan location, with a 70% reduction. The next best location is at disk three, with a 61% reduction in vibration. While the least optimum location for control of the first mode of vibrations is the bearing location, there is still a 48% reduction in vibrations over the case with no damper.

The corresponding forced response predictions are shown in Figure 10. There is a predicted 84% reduction when the damper is at the midspan and an 81% reduction when the damper is at disk three. Also there is a 34% predicted reduction when the damper is at the bearing.

A summary of the overall measured responses at the first mode is shown graphically in Figure 11 with $K_g = 2.5$. This figure shows the effect of the damper at various locations on the first mode response. It can also be noted that the vibration reduction approaches a minimum level as the damping is increased.

CONCLUSIONS

Overall, the magnetic damper achieves the desired result of a large reduction of first mode vibration at the center of the rotor. The largest reduction is 82% with the damper in the optimum location near the rotor center. These results indicate that even less than optimum placement or less than optimum control parameter setting values can produce very significant vibration reductions. This is very encouraging for the potential use of magnetic dampers in industrial applications.

It can also be noted, however, that there is a limit to the vibration reduction which can be attained by a single damper in the machine. Beyond a certain level, even a large increase in the stiffness and damping of the damper essentially produces very little further reduction of vibrations.

Generally, the agreement between the theoretical modeling of the shaft/damper system compared to the measured results is good. The magnitudes are close and the trends in the results are consistent. This indicates that the design of magnetic dampers, done on a theoretical basis before construction, has a high probability of success.

APPENDIX A
ACTIVE MAGNETIC DAMPER

This Appendix briefly discusses basic electromagnetic theory relating to the force and control of a magnetic damper. For an active magnetic damper there are four electromagnets located radially around the shaft. For the vertical direction there would be an identical top and bottom magnet and the force is

$$F_{total} = 2F_{g_{(top)}} - 2F_{g_{(bottom)}} = \frac{\mu_o AN^2 i_t^{\,2}}{h^2} - \frac{\mu_o AN^2 i_b^{\,2}}{h^2} \qquad (1)$$

In a damper, for steady state conditions,

$$i_t = i_b$$

The total force or load capacity in a magnetic damper is thus equal to zero.

$$F_{total} = W = 0$$

This, of course, would not be true in a magnetic bearing.

In an electromagnetic damper, two independent parameters can change -- position, x, and current, i. Define the position and current stiffness as

$$K_y = -\frac{\Delta F}{\Delta y} = \text{Position Stiffness}$$

$$K_i = -\frac{\Delta F}{\Delta i} = \text{Current Stiffness}$$

The gap thickness and current expressions are

$$h = h_s - \Delta y$$
$$i = i_s + \Delta i$$

for small changes about the steady state. The total force expression, Equation (1), becomes

$$F_{total} = \left[\frac{\mu_o AN^2 (i_t+\Delta i)^2}{(h_s - \Delta y)^2}\right] - \left[\frac{\mu_o AN^2 (i_b-\Delta i)^2}{(h_s + \Delta y)^2}\right]$$

or approximating by the binomial expansion,

$$F_{total} = \frac{\mu_o A N^2 i_t^2}{h_s^2}\left(1+ 2\frac{\Delta y}{h_s} + 2\frac{\Delta i}{i_s}\right) - \frac{\mu_o A N^2 i_b^2}{h_s^2}\left(1- 2\frac{\Delta y}{h_s} - 2\frac{\Delta i}{i_b}\right)$$

For steady state conditions,

$$i_t = i_b = i_s$$

so the total force equation reduces to

$$F_{total} = \frac{\mu_o A N^2 i_s^2}{h_s^2}\left(\frac{4\Delta y}{h_s} + \frac{4\Delta i}{i_s}\right)$$

The two stiffnesses K_y and K_i can now be obtained.

First setting Δi to zero,

$$F = W - K_y \Delta y = \frac{\mu_o A N^2 i_s^2}{h_s^2}\left(\frac{4\Delta y}{h_s}\right)$$

Recalling that W = zero for a damper, the total positive stiffness is

$$K_y = - \frac{4\mu_o A N^2 i_s^2}{h_s^3} \qquad (2)$$

Second, setting Δy to zero,

$$F = W - K_i \Delta i = \frac{\mu_o A N^2 i_s^2}{h_s^2}\left(\frac{4\Delta i}{i_s}\right)$$

The total current stiffness is,

$$K_i = - \frac{4\mu_o A N^2 i_s}{h_s^2} \qquad (3)$$

Both the position and current stiffnesses for the combination top and bottom electromagnets are simply two times the position and current stiffnesses for a single electromagnet, respectively.

The purpose of the electronic controller is to condition the position voltage signals from the proximitor probes and feed back the correct amount and phase of current to the magnets for optimum control of the rotor. The stiffness of the electromagnet damper is determined by the controller and can be varied by changing the proportional gain (K_g) of the controller. The damping of the electromagnetic damper is also determined by the controller. The position voltage signal from the proximitor probes is electronically differentiated so that the damping can be determined by the amount of velocity or rate signal present. The damping can be varied by changing the rate gain (K_r) of the controller.

A block diagram for the controller is shown in Figure 12. A feedback control diagram of the entire magnetic damper is shown in Figure 13. The transfer function for the electronics from the sensor amplifier through the position and current amplifier is

$$G(s) = \frac{K_t K_a K_p [K_g + (K_g + K_r) RCs] (s + 1/\tau_2)}{(1+\tau_1 s)(s+1/\tau_3)(1+RCs)} \qquad (4)$$

Finally, the total transfer function for the magnetic damper is

$$\frac{y}{F_{ext}} = \frac{\frac{1}{Ms^2 + K_y}}{1 + \frac{K_i\, G(s)}{Ms^2 + K_y}}$$

Simplifying

$$\frac{y}{F_{ext}} = \frac{1}{Ms^2 + K_y + K_i\, G(s)} \qquad (5)$$

It is easily seen that adjustment of controller proportional and rate gains (K_g and K_r) are used to adjust the stiffness and damping of the magnetic damper.

An effective damper stiffness and damping can also be obtained. The transfer function for an equivalent mass-spring-damper system is

$$\frac{y}{F_{ext}} = \frac{1}{Ms^2 + c_{eq} s + K_{eq}}$$

Equating this expression with Equation (5) gives

$$K_{eq} = K_y + K_i \mathrm{Re}\{G(j\omega)\}$$

$$c_{eq} = \frac{-K_i \mathrm{Im}\{G(j\omega)\}}{\omega} \qquad (6)$$

where s has been replaced by $j\omega$ for synchronous vibrations.

APPENDIX B
DETERMINATION OF DAMPER DYNAMIC PROPERTIES

A single mass rotor as shown in Figure 14 was used to experimentally evaluate the damping and stiffness characteristics of the magnetic damper for various settings of rate gain (K_r) and proportional gain (K_g). The effective stiffness of the damper is determined by the proportional gain (K_g) setting only. The effective damping of the magnetic damper is determined primarily by the rate gain (K_r) setting, but is also affected by the proportional gain (K_g) setting.

A rotor model of the single mass rotor was established, including support bearing characteristics, shaft bow, and unbalance in the rotor. The support bearings had a vertical stiffness of 4,030,000 N/m (23,000 lb/in) and a vertical damping of 10,000 N-sec/m (57 lb-sec/in). This model was used in a forced response program and the predicted response was compared to experimentally measured rotor response. Various values of stiffness and damping were added to the rotor model at the electromagnetic damper location until predicted response (i.e. frequency and amplitude of the first mode response) matched the experimental rotor response to within approximately 5%. An example of experimental data and its corresponding or "matching" calculated response is shown in Figure 15 for the case when the proportional gain (K_g) equals 2.5 and the rate gain (K_r) equals 2.0. In this manner stiffness and damping characteristics for the electromagnetic damper were determined for various values of rate gain (K_r) and proportional gain (K_g). The stiffness values are listed in Table 1 and the damping values are listed in Table 2.

The damping and stiffness characteristics of the magnetic damper determined in this manner were used in the rotor model of the 3-mass rotor for forced response calculations.

REFERENCES

1. Kludt, F. H., and Salamone, D. J., "Rotor Dynamics Modification of an Eight Stage Compressor for Safety/Reliability Improvement," Twelfth Turbomachinery Symposium, Texas A&M University, November 15-17, 1983, pp 81-96.

2. Allaire, P. E., Stroh, C. G., Flack, R. D., Kocur, J. A., and Barrett, L. E., "Subsynchronous Vibration Problem and Solution in Multistage Centrifugal Compressor," Proc. of 16th Turbomachinery Symposium, Spnosored by Texas A&M University, Dallas, TX, October 26-29, 1987.

3. Nicholas, J. C., and Barrett, L. E., "The Effect of Bearing Support Flexibility on Critical Speed Prediction," ASLE Trans., Vol. 29, No. 3, pp. 329-338, April 1986.

4. Foster, E. G., Kulle, V. and Peterson, R. A., "The Application of Active Magnetic Bearings to a Natural Gas Pipeline Compressor," ASME Gas Turbine Conference, Paper 86-GT-61, Dusseldorf, June, 1986.

5. Hustak, J. F., Kirk, R. G., and Schoeneck, K. A., "Analysis and Test Results of Turbocompressors Using Active Magnetic Bearings," Presented at ASLE Annual Meeting, Toronto, Ontario, Canada, May 12-15, 1986.

6. Allaire, P. E., Lewis, D. W., and Jain, V. K., "Feedback Control of a Single Mass Rotor on Rigid Supports," Journal of the Franklin Institute, Vol. 312, 1981, pp. 1-11.

7. Allaire, P. E., Lewis, D. W., and Knight, J. D., "Active Vibration Control of a Single Mass Rotor on Flexible Supports," Journal of the Franklin Institute, Vol. 315, 1983, pp. 211-222.

8. Nikolajsen, J. L., Holmes, R., and Gondhalekar, V., "Investigation of an Electromagnetic Damper for Vibration Control of a Transmission Shaft," The Institution of Mechanical Engineers, 1979, Vol. 193, No. 31, pp. 331-336.

9. Gondhalekar, V. and Holmes, R., "Design of an Electromagnetic Bearing for the Vibration Control of a Flexible Transmission Shaft," Rotor Dynamics Instability Problems in High Performance Turbomachinery, Texas A&M University, May 1984.

10. Humphris, R. R., Kelm, R. D., Lewis, D. W., and Allaire, P. E., "Effect of Control Algorithms on Magnetic Journal Bearing Properties," J. of Engr. for Gas Turbines and Power. Trans. ASME, Vol. 108, October 1986, pp. 624-632.

11. Allaire, P. E., Humphris, R. R., and Kelm, R. D., "Dynamics of a Flexible Rotor in Magnetic Bearings," Proc. of Rotordynamic Instability Problems in High-Performance Turbomachinery, June 2-4, 1986, NASA Conference Publication 2443, pp. 419-430.

12. Allaire, P. E., Humphris, R. R., and Barrett, L. E., "Critical Speeds and Unbalance Response of a Flexible Rotor in Magnetic Bearings," Proc. of European Turbomachinery Symposium, October 27-28, 1986.

13. Allaire, P. E., Humphris, R. R., and Imlach, J., "Vibration Control of Flexible Rotors with Magnetic Bearing Supports," AFOSR/ARO Conference, Nonlinear Vibrations, Stability, and Dynamics of Structures and Mechanisms, Virginia Tech, Blacksburg, Virginia, March 23-25, 1987.

14. Allaire, P. E., Humphris, R. R., Kasarda, M. E. F., and Koolman, M. I., "Magnetic Bearing/Damper Effects on Unbalance Response of Flexible Rotors," Proc. AIAA Conference, Philadelphia, PA, August 10-14, 1987.

15. Keith, F. J., Williams, R. D., Allaire, P. E., and Schafer, R. M., "Digital Control of Magnetic Bearings Supporting a Multimass Flexible Rotor," Presented at NASA Conference on Magnetic Suspension Technology, NASA Langley, February 2-4, 1988.

Table 1 - Horizontal and Vertical Stiffness Values of the Magnetic Damper at Approximately 2500 RPM (41.7 Hz).

Proportional Gain (K_g)		0	2.5	5.0	7.5	10.0
K_x	(N/m)	-35,000	44,000	190,000	210,000	260,000
	(lb/in)	(-200)	(250)	(1100)	(1200)	(1500)
K_y	(N/m)	-35,000	70,000	175,100	210,100	263,000
	(lb/in)	(-200)	(400)	(1000)	(1200)	(1500)

Table 2 - Horizontal and Vertical Damping Values (lb-sec/in) of the Magnetic Damper at 2500 RPM (41.7 Hz)

K_r =	0.0	2.0	5.0	10.0
K_g	$\frac{N\text{-}sec}{m}(\frac{lb\text{-}sec}{in})$	$\frac{N\text{-}sec}{m}(\frac{lb\text{-}sec}{in})$	$\frac{N\text{-}sec}{m}(\frac{lb\text{-}sec}{in})$	$\frac{N\text{-}sec}{m}(\frac{lb\text{-}sec}{in})$
0.0	C_x=33(C_x=.19) C_y=30(C_y=.17)	-	-	-
2.5	U	C_x=49(C_x=.28) C_y=32(C_y=.18)	C_x=100(C_x=.62) C_y= 84(C_y=.48)	$C_x\approx$150($C_x\approx$.85) $C_y\approx$120($C_y\approx$.70)
5.0	U	U	C_x= 51(C_x=.29) C_y= 42(C_y=.24)	-
7.5	U	U	U	C_x= 47(C_x=.27) C_y= 47(C_y=.27)
10.0	U	U	U	U

U = Unstable

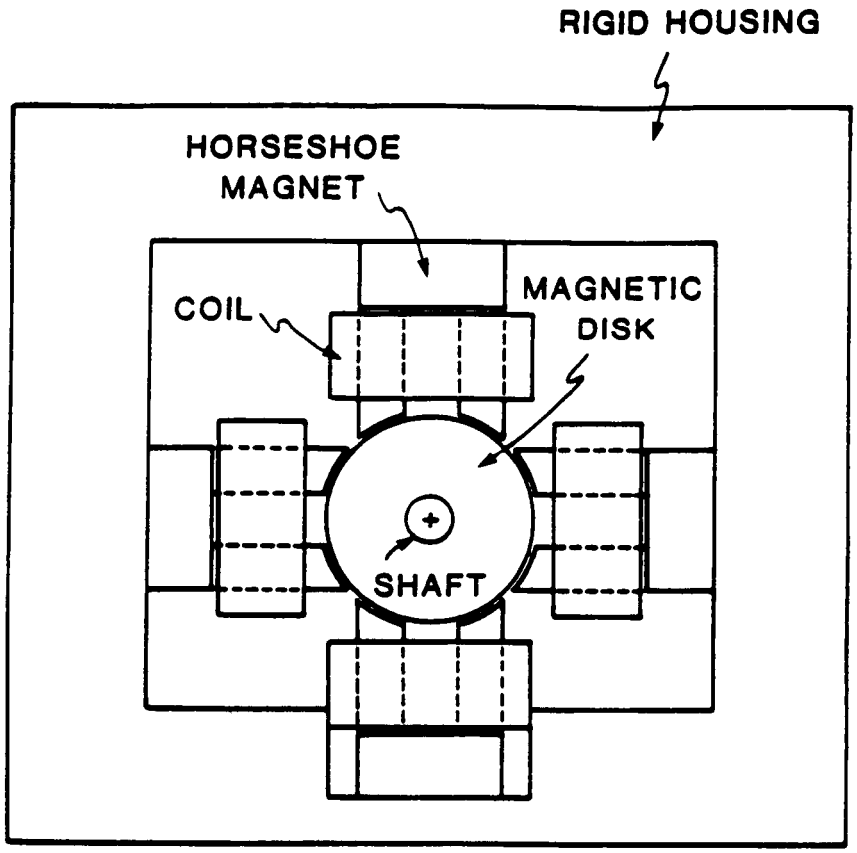

Figure 1 Magnetic Damper Model

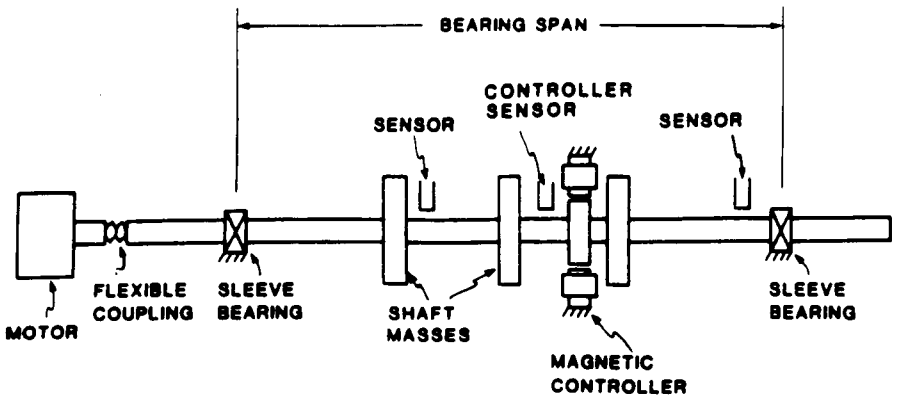

DAMPER AT MIDSPAN

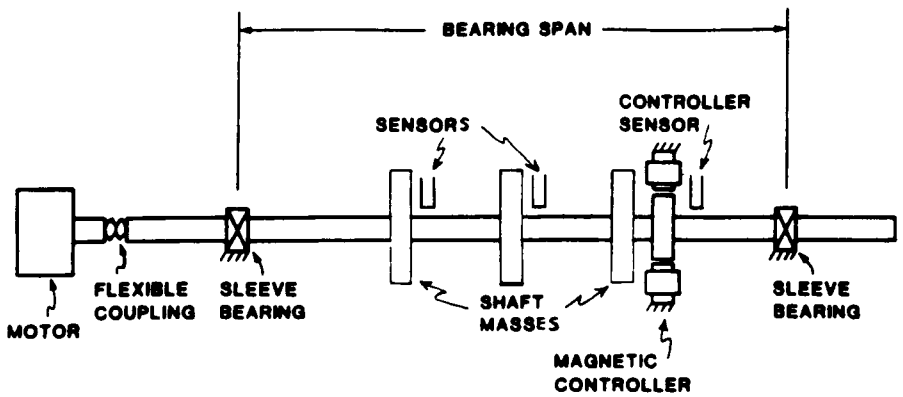

DAMPER AT DISK THREE

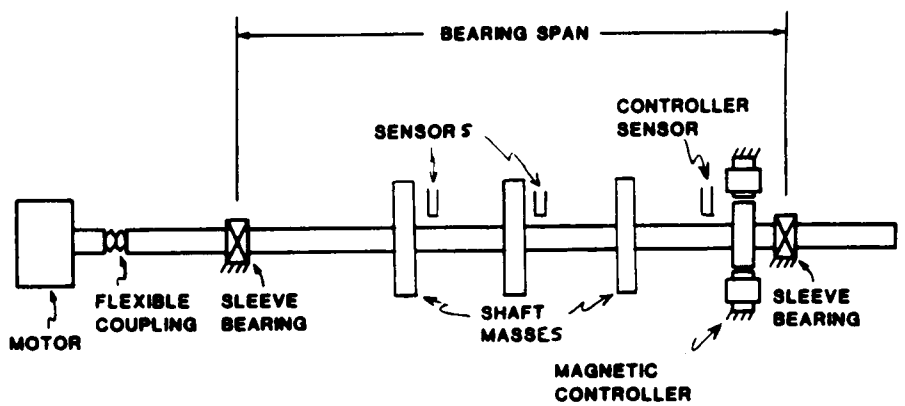

DAMPER AT BEARING

Figure 2 Schematic of 3-Mass Rotor with Magnetic Damper at Three Different Locations (Not to Scale)

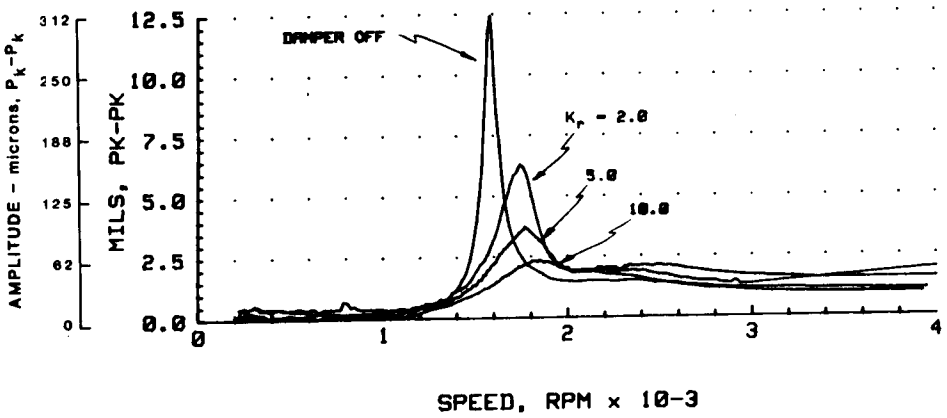

Figure 3 Experimental Results for the Damper at Midspan (Increasing Rate Gain (K_r)) at the Vertical Midspan Probe - K_g = 2.5

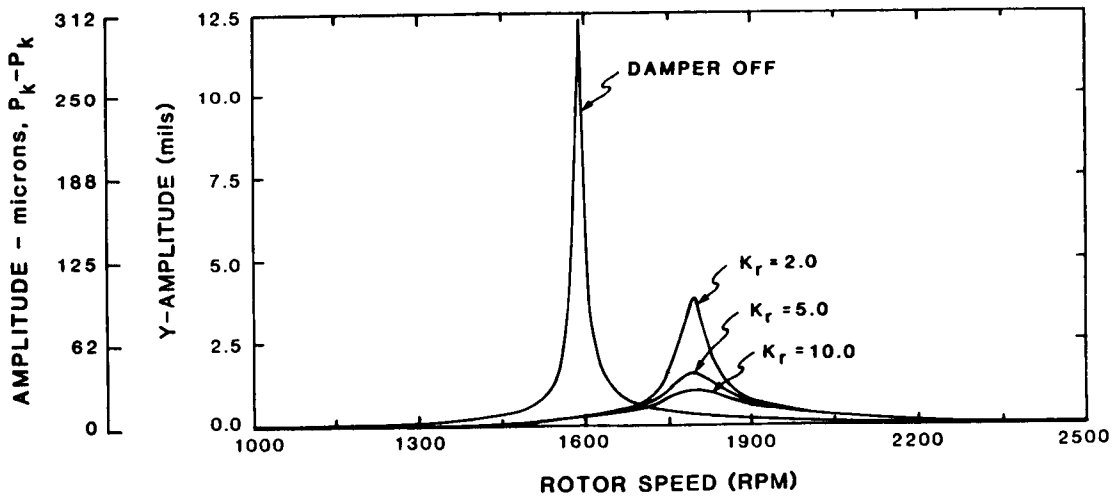

Figure 4 Forced Response Program Predictions for Damper at Midspan (Increasing Rate Gain (K_r)) at Vertical Midspan Probe - K_g = 2.5

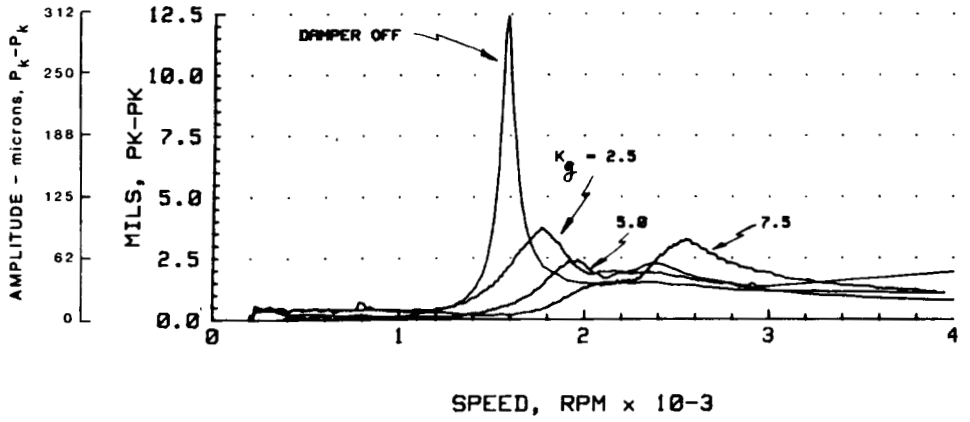

Figure 5 Experimental Results for the Damper at Midspan (Increasing Proportional Gain (K_g)) at the Vertical Midspan Probe - K_r = 5.0

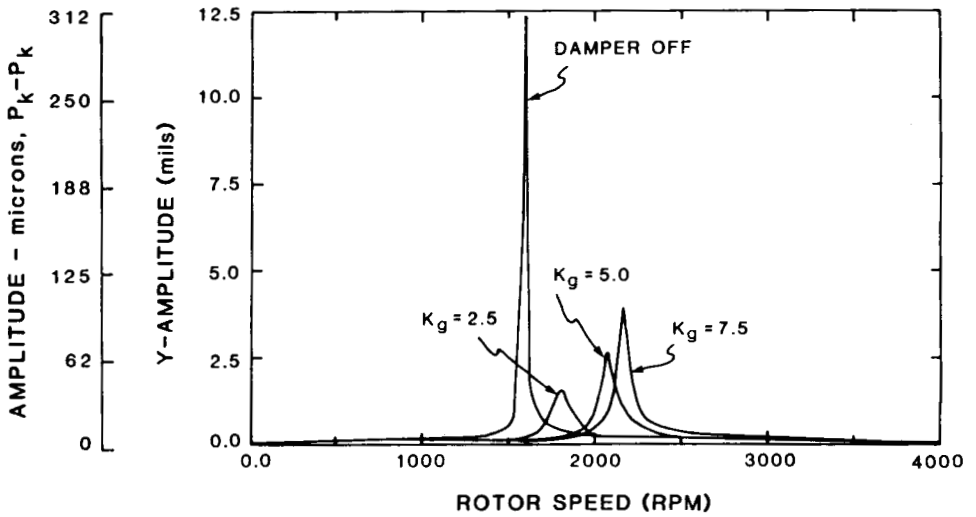

Figure 6 Forced Response Program Predictions for Damper at Midspan (Increasing Proportional Gain (K_g)) at Vertical Midspan Probe - K_r = 5.0

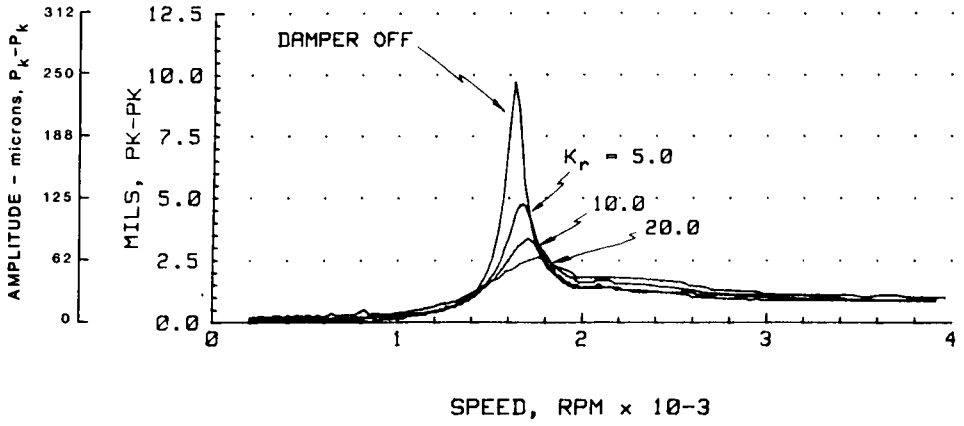

Figure 7 Experimental Results for the Damper at Disk Three (Increasing Rate Gain (K_r)) at the Vertical Midspan Probe - K_g = 2.5

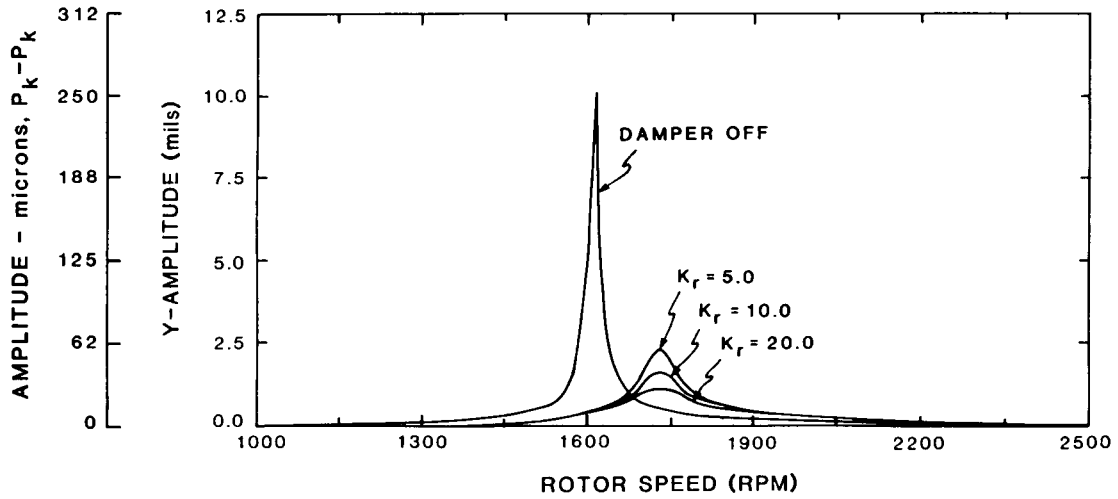

Figure 8 Forced Response Program Predictions for Damper at Disk Three (Increasing Rate Gain (K_r)) at Vertical Midspan Probe - K_g = 2.5

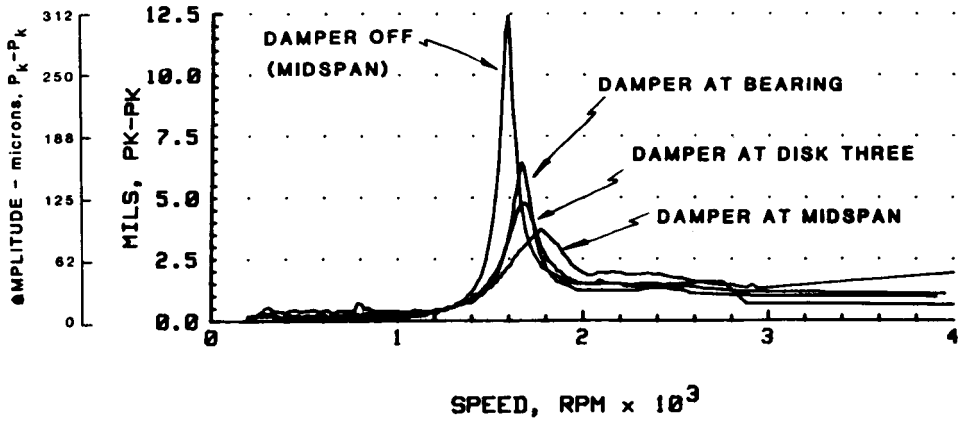

Figure 9 Experimental Results at Vertical Midspan for the Damper at Three Locations (Proportional Gain (K_g) equal to 2.5, Rate Gain (K_r) equal to 5.0)

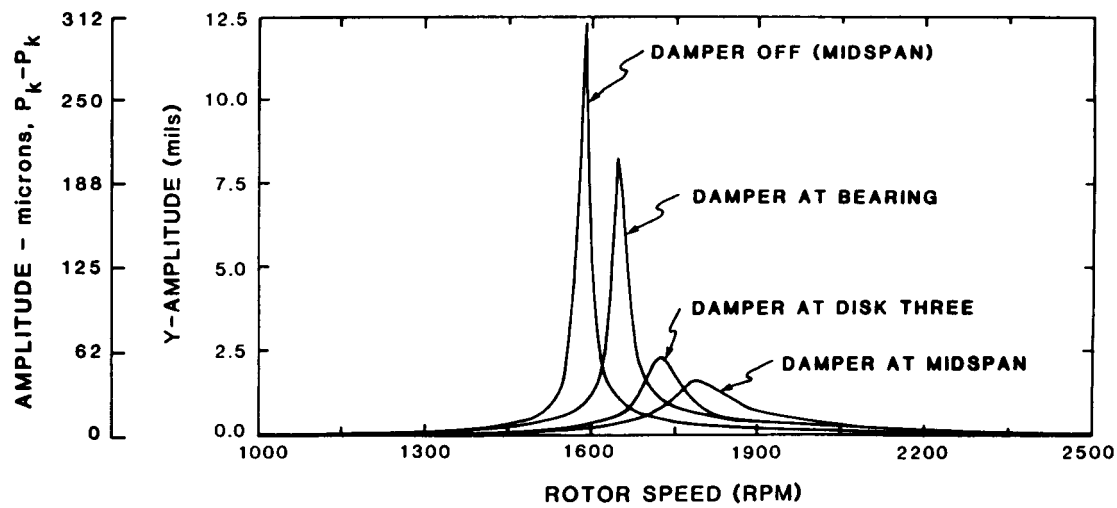

Figure 10 Forced Response Predictions for the Damper at Three Locations (Proportional Gain (K_g) equal to 2.5, Rate Gain (K_r) equal to 5.0)

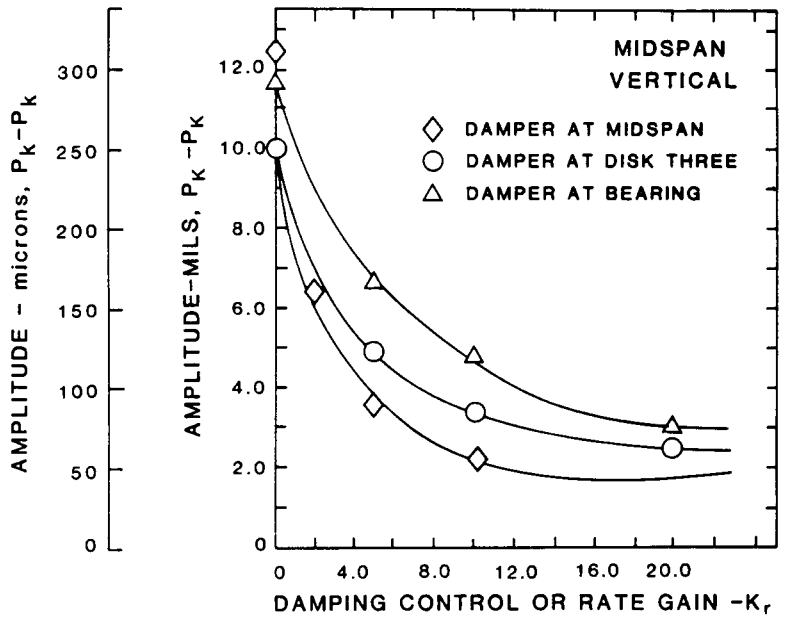

Figure 11 Response Amplitude at First Mode vs. Rate Gain (Damper at Midspan, Disk Three, and Bearing Location)

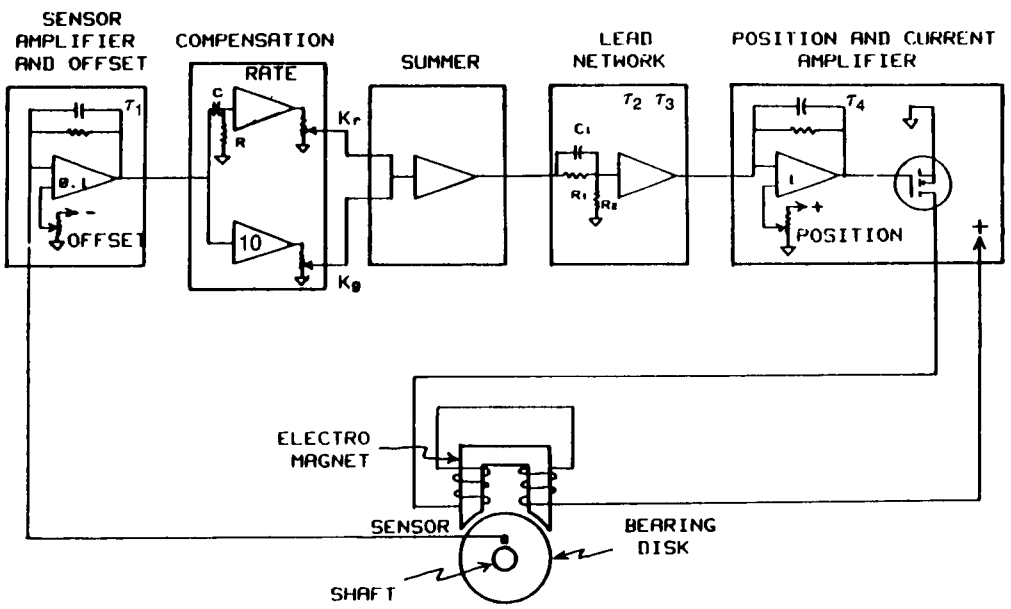

Figure 12 Block Diagram of Control Circuit

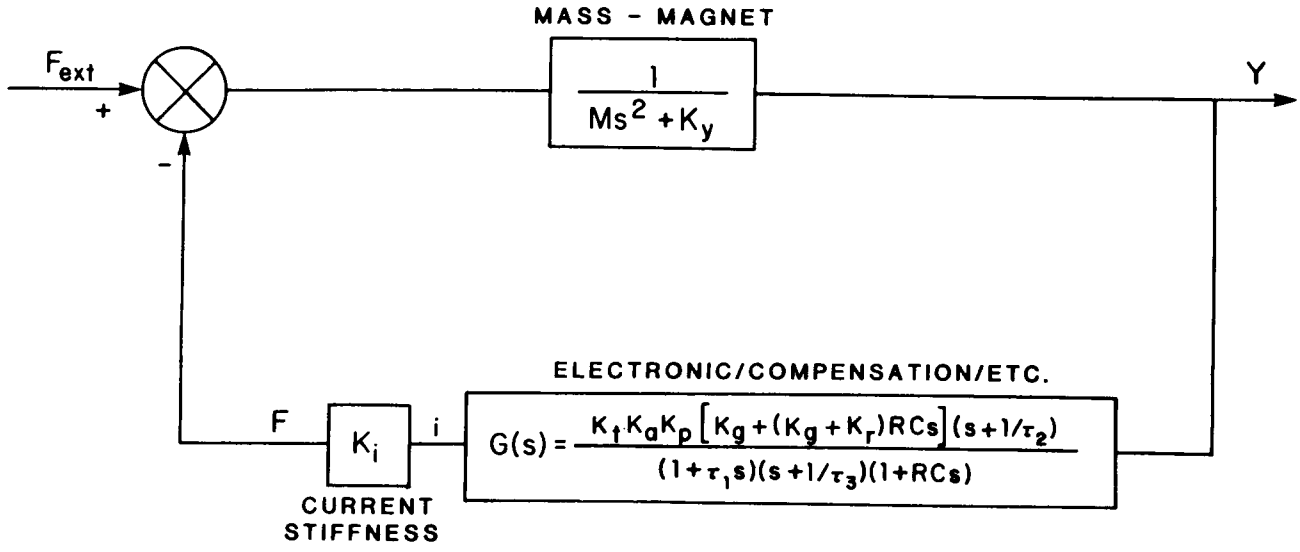

Figure 13 Diagram of Magnetic Damper System for Controller

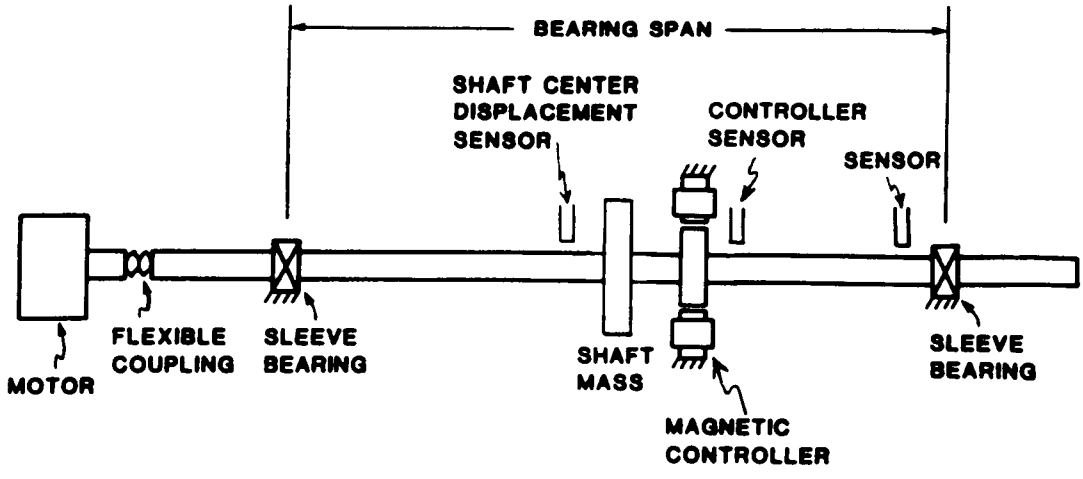

Figure 14 Schematic of Single Mass Rotor with Magnetic Damper (Not to Scale)

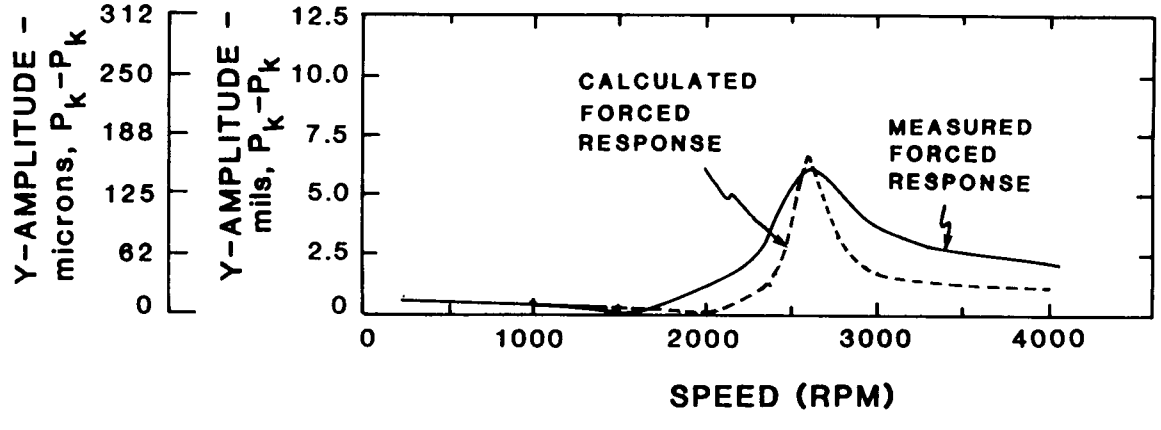

Figure 15 Comparison of Calculated and Experimentally Measured Forced Response